Materials Science & Engineering C 81 (2017) 224–235

Contents lists available at ScienceDirect

Materials Science & Engineering C

journal homepage: www.elsevier.com/locate/msec

Polyethyleneimine grafted short halloysite nanotubes for gene delivery

Zheru Long, Jun Zhang, Yan Shen, Changren Zhou, Mingxian Liu*

Department of Materials Science and Engineering, Jinan University, Guangzhou 510632, China

ARTICLE INFO

Keywords:
Halloysite nanotubes
Polyethyleneimine
Grafting
Biocompatibility
Transfection

ABSTRACT

Inorganic nanoparticles have attracted much attentions in gene delivery because of their desirable characteristics including low toxicity, well-controlled characteristics, high gene delivery efficiency, and multi-functionalities. Here, natural occurred halloysite nanotubes (HNTs) were developed as a novel non-viral gene vector. To increase the efficiency of endocytosis, HNTs were firstly shortened into an appropriate size (~200 nm). Then polyethyleneimine (PEI) was grafted onto HNTs to bind green fluorescence protein (GFP) labeled pDNA. The structure and physical-chemical properties of PEI grafted HNTs (PEI-g-HNTs) were characterized by various methods. PEI-g-HNTs show lower cytotoxicity than PEI. PEI-g-HNTs are positively charged and can bind DNA tightly at designed N/P ratio from 5:1 to 40:1. PEI-g-HNTs/pDNA complexes show much higher transfection efficiency towards both 293T and HeLa cells compared with PEI/pDNA complexes at the equivalent N/P ratio. The transfection efficiencies of PEI-g-HNTs/pDNA complex towards HeLa cell can reach to 44.4% at N/P ratio of 20. PEI-g-HNTs/pDNA complexes possess a higher GFP protein expression than PEI/pDNA from simple western immunoblots. So, PEI-g-HNTs are potential gene vectors with good biocompatibility and high transfection efficiency, which have promising applications in cancer gene therapy.

1. Introduction

Gene therapy is the therapeutic delivery of nucleic acid into a patient's cells as a drug to treat disease [1]. The effect of gene therapy largely depends on an appropriate gene delivery vector, which can carry and protect foreign genetic materials into cells where the gene can be replicated and/or expressed [2]. Although viral vectors are able to deliver nucleic acids into cell lines efficiently [3], they have strong immunogenicity, inflammatory reactions, toxicity limit and many other adverse effects [4], Non-viral vectors especially inorganic nanoparticles are attracting many attentions because of their lower immunogenic characteristic, good biosafety, and easy preparation [5]. Inorganic nanoparticles, including carbon nanotubes, magnetic nanoparticles, graphene oxide (GO), calcium phosphate and calcium carbonate nanoparticles, metal nanoparticles, have been developed into novel gene vectors that offer enhanced transfection efficacy and many other uses with minimized toxicity [6–17]. They can be chemically synthesized with the control of shape, size, and chemical properties, as well as composition [1]. Given the large size and the negative charge of nucleic acid, chemical modification of inorganic nanoparticles with functional groups or polymers is generally needed. Positively charged functional groups (usually the amide groups) or polymers, such as amino silane, polyethyleneimine (PEI), polyamidoamine (PAMAM), chitosan, are usually be employed to treat the nanoparticles before binding with DNA. For instance, PEI grafted GO exhibited enhanced chemotherapy efficacy towards HeLa cells by sequential delivery of anticancer drugs and siRNA [18]. Protamine functionalized carbon nanotubes (CNTs) could also increase the DNA internalization towards MCF-7 cell [19]. PEI functionalized CNTs/siRNA complex could cross the cell membrane efficiently and induce apoptosis and suppression in proliferation of tumor cells both *in vitro* and *in vivo* [20]. Oligonucleotide-modified gold nanoparticles exhibited high cellular uptake and protected nucleic acid from the degradation, and were nontoxic to the cells, which could be used as a tunable gene knockdown system [21]. PEI coated magnetic nanoparticles showed high transfection efficiency even towards the hard-to-transfect cells like Jurkat cells [22]. Multi-modal transfection agent based on Fe_3O_4 were also used for stem cell gene delivery, and the transfection efficiency reached to 22.3% which was significantly higher than that of PEI (12.1%) [23]. However, it is still a big challenge to select a natural nanoparticle with high transfection efficiency and good biocompatibility [24].

Halloysite nanotubes (HNTs), with a formula of $Al_2Si_2O_5(OH)_4{\cdot}nH_2O$, are novel 1D natural inorganic clay nanotubes [25]. HNTs with the characteristics of tubular nanostructure (~50 nm in outer diameter, 10–15 nm in lumen) [26,27], high stability in biological liquid, easy modification, low cost, good biocompatibility [28] and proper mechanical property. Therefore, HNTs show an active vitality in biomedical applications [29–31] and gene therapy research

* Corresponding author.
E-mail address: liumx@jnu.edu.cn (M. Liu).

http://dx.doi.org/10.1016/j.msec.2017.07.035
Received 18 May 2017; Received in revised form 17 June 2017; Accepted 13 July 2017
Available online 22 July 2017
0928-4931/ © 2017 Elsevier B.V. All rights reserved.

[32,33] in recent years. HNTs possess two types of hydroxyl groups in its inside and outsider, which can be used as active sites for functionalization [34]. Diverse drugs can be loaded into the inner tubular structure and/or the layer spaces of HNTs [25] through chemical modification and vacuum process [35,36]. For gene delivery, HNTs were firstly grafted with gaminopropyltriethoxysilane and delivered the antisense oligonucleotides towards HeLa cells [32]. Recently, a progress in capture of tumor cells based on HNTs rough surfaces and chitosan grafted HNTs (HNTs-g-CS) as a drug delivery of curcumin or adriamycin for enhancing anticancer efficacy were achieved [25,37]. All the existing studies indicate that HNTs are potential materials for anticancer drug delivery in cancer therapy.

However, the commercially available HNTs are usually inhomogeneous with a length from 100 nm to 2 μm [38]. Long nanotubes usually lead to more potent inducers of cell injury and inflammation [30]. Previous findings suggested that nanoparticle with diameter < 200 nm may be the suitable candidate to serve as a carrier for drug delivery due to their relatively high endocytosis compared with large nanoparticles [39]. Also, nanoparticles with small particle size are safer in biological applications. For example, length of the CNTs around 220 nm could phagocytosed by cells more readily and showed relatively low cytotoxity than that beyond 220 nm [40]. So, it is important to prepare homogeneous HNTs with a short length such as below 200 nm. On the other hand, the negative charges of HNTs limit their applications in gene delivery since the nucleic acid is also negatively charged. Functionalized HNTs can be achieved *via* electrostatic layer-by-layer assembling of cationic PEI, which can effectively deliver siRNA into cancer cells and noninvasively image the process simultaneously [33]. However, the dissociation of PEI layer of HNTs may quickly occur during operation process due to the water-soluble character of PEI, which will decrease the gene transfection efficacy *in vitro* and *in vivo*.

Here, PEI grafted short HNTs (PEI-g-HNTs) as a non-viral vector were developed for loading and intracellular delivery of DNA. Firstly, the ultrasonic treatment was used to cut the long HNTs into short nanotubes accordingly to the reference [38]. Then PEI was chemically grafted onto HNTs to change the surface potential into positive charges. PEI-g-HNTs was characterized with morphological and chemical analysis, and all the results suggested the successful synthesis of PEI-g-HNTs. Fig. 1 shows the preparation and cell uptake process of PEI-g-HNTs as vehicles of GFP labeled DNA. Excitingly, PEI-g-HNTs showed low cytotoxicity and dramatically increased transfection efficiency compared with PEI at established N/P ratios.

2. Experimental

2.1. Materials

Halloysite nanotubes (HNTs) were purchased from Guangzhou Runwo Materials Technology Co., Ltd., China. HNTs were purified according to the reference to remove the impurities [41]. Polyvinyl pyrrolidone (PVP K30), polyethylenimine (PEI 10 kDa), succinic anhydride (SA) 3-aminopropyltriethoxy silane (APTES), *N*-(3-dimethylaminopropyl)-*N′*-ethylcarbodiimide (EDC), and N-hydroxysuccinimide (NHS) were purchased from Aladdin. All other chemicals were used as purchased (Aladdin) without further purification. Green fluorescent protein labeled DNA (GFP-pDNA) was obtained from Prof. Ma Dong group in Jinan University. Ultrapure water from a Milli-Q water (resistivity > 18.2 MΩ·cm)) system was used in all experiments.

2.2. Shortening of HNTs

HNTs were shortened according to the previous study with slight modification [38]. The typical procedures was given below. Purified HNTs (1 g) were suspended in 50 mL of 3 wt% PVP solution by stirring for 30 min. The homogeneous suspension was sonicated for 30 min at 550 W using an ultrasonic cell disruptor (Scientz-II D, Ningbo Scientz Biotechnology Ltd., China). Then the HNTs suspension was centrifuged at 5000 rpm for 45 min using an ultracentrifuge (YNX-4000, Thermo Fisher Scientific Ltd., USA). The supernatant was transferred into another 50 mL centrifuge tube and centrifuged again at 16000 rpm for 5 min. The resulting precipitate was gathered and washed by ultrapure water and anhydrous ethanol alternately, each for three times. Finally, the short HNTs with length ~200 nm were obtained by freeze-drying at − 56 °C. The HNTs used in the following experiment were all short HNTs.

2.3. Synthesis of PEI-g-HNTs

PEI-g-HNTs were synthesized according to the previous study with modification [42]. Firstly, the surface hydroxyl groups of HNTs were transferred into amide groups by reacting with APTES. Acetic acid was added into 150 mL ethyl alcohol (95%) to adjust the pH to 4. Afterwards, 20 g KH-550 was added into the solution under stirring at 40 °C. 2 g HNTs were added into the solution by stirring for 30 min and ultrasonically treated for another 30 min to obtain good dispersion state

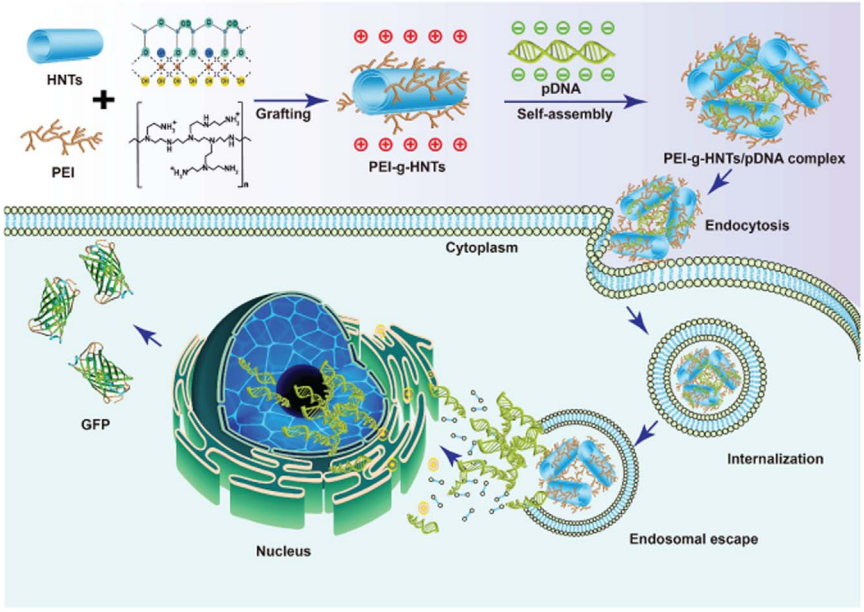

Fig. 1. Schematic illustration of the processes of preparation and structure of PEI-g-HNTs/pDNA complex and its delivery of the pDNA to the cells.

of HNTs. Afterwards, the mixture was reacted for 24 h under stirring at 80 °C. The product of amide groups grafted HNTs (HNTs-NH_2) was washed by ultrapure water and anhydrous ethanol alternately, each for three times, and then dried by freezer dryer. 1 g succinic anhydride and 0.5 g HNTs-NH_2 were reacted in 50 mL *N,N*-dimethylformamide (DMF) with stirring and ultrasonic treatment at room temperature for 24 h. The carboxyl grafted HNTs (HNTs-COOH) were washed by anhydrous ethanol and ultrapure water alternately. 0.2 g HNTs-COOH and 0.67 g EDC were added into 20 mL ultrapure water, then stirred and ultrasonic treated for 10 min. 0.4 g NHS and 0.5 g PEI were added into the mixture. After 24 h, PEI-g-HNTs were obtained by centrifuging, washed by anhydrous ethanol and ultrapure water alternately, each for five times, and dried by freezer dryer.

2.4. Characterization of PEI-g-HNTs

2.4.1. Scanning electron microscope (SEM)

A certain amount of raw HNTs and short HNTs were dispersed in ultrapure water under stirring and ultrasonic treatment. Then the dispersion was dropped and dried on glass sheet substrate. The samples were observed by SEM (Ultra-55, Carl Zeiss Jena Ltd., Germany) at an accelerating voltage of 5 kV.

2.4.2. Transmission electron microscopy (TEM)

The dilute HNTs and PEI-g-HNTs ethanol dispersions were dropped and dried on carbon film supported copper grid. The samples were observed using TEM (JEM-2100F, JEOL Ltd., Japan) under an accelerating voltage of 100 kV.

2.4.3. Dynamic light scattering (DLS)

The size of raw HNTs and short HNTs was tested by a Nano-ZS instrument (Malvern Instruments Ltd., UK). The size of PEI-g-HNTs/pDNA complexes (N/P = 20) was measured at the pH of 5.4, 7.4, 9. Meanwhile, the size of PEI-g-HNTs/pDNA complexes dispersed in ultrapure water solution at N/P ratios of 5, 10, 20, 40 was compared. HNTs aqueous dispesion with concentration of 0.05 wt% was measured.

2.4.4. Atomic force microscopy (AFM)

Morphology of the HNTs and PEI-g-HNTs was observed with a multimode atomic force microscopy instrument (Bioscope Catylyst Nanoscope-V, broker, Instruments Ltd., USA) which mounted on an inverted optical microscope (IX51, Olympus, Tokyo, Japan). The images were captured with Tap150-Al-G silicon AFM probes (budgets sensors) in ScanAsyst mode (k = 5 N/m, scanning speed was 1 Hz, resonance frequency 150 kHz in air). The experiment was performed at room temperature. Nanoscope analysis soft was used to analyze the diameters of HNTs and PEI-g-HNTs.

2.4.5. Qualitative analysis of the amine groups

Qualitative analysis of amine group on the PEI-g-HNTs was carried out by ninhydrin colorimetric assay [43]. Samples were diluted in ultrapure water, then mixed with equal volume of ninhydrin solution (500 mL of 0.2% w/v in 0.1 M buffer phosphate, pH = 9), and the mixture was heated in a boiling water bath for 20 min. Samples were cooled to room temperature and then centrifuged. The absorbance of supernatants was measured at 570 nm on a UV–visible spectrophotometer (UV-2550, Shimadzu Instrument Ltd., Suzhou, China).

2.4.6. UV–Vis spectra

The UV–Vis spectra of HNTs, pDNA and PEI-g-HNTs/pDNA complexes (N/P = 20) were measured by UV–visible spectrophotometer (UV-2550, Shimadzu Instrument Ltd., Suzhou, China).

2.4.7. X-ray diffraction (XRD)

XRD analysis was tested with X-ray diffractometer (MiniFlex-600, Rigaku Corporation, Japan).

2.4.8. ξ-Potential analysis

Zeta potential of PEI-g-HNTs/pDNA complexes (N/P = 20) was measured at the pH of 5.4, 7.4, 9. Meanwhile, Zeta potential of PEI-g-HNTs/pDNA complexes dispersed in ultrapure water solution at N/P ratios of 5, 10, 20, 40 was compared. Zeta potential of the HNTs, PEI, and PEI-g-HNTs aqueous dispersion was measured using a Nano-ZS instrument (Malvern Instruments Ltd., England). The concentration of the dispersions was 5×10^{-2} wt%.

2.4.9. Fourier transform infrared spectroscopy (FTIR)

The FTIR spectra of the HNTs samples were tested using Thermo FTIR (Nicolet iS50, Thermo Fisher Scientific Ltd., USA). Before measurement, the samples were pelleted with potassium bromide. Twenty-two consecutive scanning were taken and stored their average. Spectra were taken from 4000 to 400 $cm^{-1.}$ The resolution of the wavenumber was 2 cm^{-1}.

2.4.10. Thermogravimetric analysis (TGA)

TGA was handled with TGA instrument (TG209F3-ASC, Netzsch Ltd., Germany) from 30 °C to 700 °C at a heating rate of 10 °C/min under N_2 atmosphere. This experiment was used to compare the weight loss behavior of HNTs and PEI-g-HNTs, which could be used to calculate the grafting percent. The percentage of grafting of PEI on PEI-g-HNTs was calculated by the following equation.

$$\text{Grafting}\,(\%) = m/M \times 100\%$$

where m (g) is the weight of organics grafted on HNTs, M (g) is the weight of PEI-g-HNTs [25].

2.4.11. X-ray photoelectron spectroscopy (XPS)

XPS analysis was conducted by XPS instrument (ESCALAB250Xi, Thermo Fisher Scientific Ltd., USA). The atoms of Al, Si, C, N, and O were detected.

2.4.12. Barrett-Joyner-Halenda (BJH) methods

BJH pore analysis was implemented by automated surface area and pore size analyzer (TriStar II-3020, Micromeritics Instrument Corporation, USA). The adsorption and desorption curves were obtained simultaneously.

2.5. Cells and cell culture conditions

Human cervical epithelial adenocarcinoma cells (HeLa), and 293T cells were cultured in DMEM supplemented with 10% fetal bovine serum (FBS), 1% antibiotic/antimicrobial at 37 °C under 5% CO_2 humidified atmosphere. The cells were purchased from the Laboratory Animal Center of Sun Yat-Sen University.

2.6. Biocompatibility of PEI-g-HNTs/pDNA

2.6.1. AO/EB staining assay

HeLa and 293T cells (1×10^4 cells/well) were seeded in 96-well plate for 24 h to allow attachment, then a series of N/P ratios of PEI/pDNA and PEI-g-HNTs/pDNA complexes (5, 10, 20, 40) containing 0.2 μg pDNA per well were added for 24 h. The cells were stained by acridine orange/ethidium bromide (AO/EB) double fluorescent dyes and observed with fluorescence microscope (XDY-2, Guangzhou Liss Optical Instrument Ltd., China) [44].

2.6.2. Cell counting kit-8 (CCK-8) assays

HeLa and 293T cells (1×10^4 cells/well) were seeded in a 96-well plates and cultured at 37 °C in 5% CO_2 for 24 h, and subsequently treated with the polyplexes containing 0.2 μg pDNA per well at various N/P ratios (5, 10, 20, 40) for another 24 h. The measurements of each ratio were conducted in four parallel groups. Afterwards, cells were washed with PBS twice and then replaced with 100 μL fresh medium.

Finally, 10 μL CCK-8 reagents were added into each well and incubated for another 4 h. The absorbance at 450 nm was recorded by a microplate reader. Cell viability was the ratio of absorbance of the sample and the control group.

2.6.3. Hemocompatibility assays

2 mL fresh rabbit blood was added into 10 mL PBS solutions, then the supernatant liquid was abandoned after centrifuging the mixture solution for 3 times. The red blood cells (RBCs) were collected and added into 3 mL PBS solution (RBCs suspension). PEI and PEI-g-HNTs were mixed with 0.2 μg pDNA (N/P = 20) by a vortex mixer and then incubated for 30 min at room temperature, then the total volume of complexes were adjusted with PBS to 500 μL, respectively. PEI and PEI-g-HNTs PBS solution were added into 50 μL RBCs suspension. Equivalent ultrapure water and PBS solution were added as the positive control group and the negative control group, respectively. All the samples were incubated at 37 °C for 1 h then centrifuged at 1000 rpm for 5 min. Additionally, supernatant liquid of PEI-g-HNTs group was centrifuged at 15000 rpm for 5 min to eliminate the effect of PEI-g-HNTs. The absorbance at 570 nm of supernatant liquid was measured with microplate reader. The hemolysis rate was calculated as follows equation.

$$\text{Hemolysis rate } (\%) = \frac{\text{sample absorbance} - \text{negative control}}{\text{positive control} - \text{negative control}} \times 100\%$$

2.7. Gel electrophoresis

Agarose gel electrophoresis retardation assay was applied to examine the pDNA loading ability of PEI and PEI-g-HNTs. A constant amount of 0.2 μg pDNA was used. The PEI/pDNA and PEI-g-HNTs/pDNA complexes (N/P = 0, 1, 2, 5, 10, 20 and 40) were loaded onto a 0.6 g agarose gel which was dissolved in 60 mL TAE buffer (40 mM Tris-acetate, 1 mM EDTA) containing 3 μL Ethidium Bromide and electrophoresed at 100 V for 30 min. Then pDNA was then visualized using an UV transilluminator (CUV-10, Qin Xiang Scientific Instrument Co., Ltd. Shanghai).

2.8. In vitro transfection

293T cells were seeded in DMEM supplemented with 10% FBS and 1% antibiotic/antimicrobial at a density of 8×10^4 cells/well in a 6-well plate for 24 h at 37 °C, under 5% CO_2 humidified atmosphere. PEI or PEI-g-HNTs were mixed with 1 μg pDNA (N/P = 20), 12.4 μL $CaCl_2$, and 84.6 μL ultrapure water by a vortex mixer and incubated for 30 min at room temperature. Afterwards, 100 μL 2 × HBS (11.92 g/L Heprs-NaOH, 0.75 g/L KCl, 16.36 g/L NaCl, 2.16 g/L dextrose, and 0.21 g/L Na_2HPO_4) was added to form a homogeneous solution. 293T cells were incubated with the transfection solution for 8 h at 37 °C under 5% CO_2 atmosphere. Then the transfection solution was removed and then washed with PBS thoroughly, and the cells were cultured with DMEM culture media for an additional 72 h. The transfection efficiency was then quantified by flow cytometry (FACS Gallios, Beckman, USA).

HeLa cells were transferred to 96-well plate at a density of 1×10^5 cells/well. EK transfer buffer (60 μL) was added as a buffer solution. Then PEI and PEI-g-HNTs mixed with pDNA (0.2 μg per well) at different N/P ratio (5, 10, 20, 40) were added into the cell culture plates and incubated for 30 min. Afterwards, the HeLa cells were treated with electric transfection instrument (X-Porator H1, Yida Biological Technology Co., Ltd. China) with 200 V voltage and then cultured with DMEM in 24-well plate for 72 h. The transfection efficiency was then quantified by flow cytometry (FACS Gallios, Beckman, USA).

2.9. Simple western blot analysis

The simple western immunoblots were performed to measure the GFP protein expression level in cells after transfection [45]. In simple western immunoblots analysis, western blot analysis was performed using a capillary-based automated system. The simple western immunoblots were performed using the Wes 12–230 kDa Master Kit with Split Buffer (PS-MK16) according to the manufacturer's standard instruction. GFP mouse monoclonal antibody (Affinity, T0005) was used as the primary antibody at a dilution proportion of 1:50 and the secondary antibodies from ProteinSimple were used neat. In brief, transfected cells were washed with PBS, and then re-suspended in 80 mL of lysis buffer, the supernatant was collected by centrifugation for 5 min at 6000 r/min. For obtaining standard curve, 100 g albumin from bovine serum (BSA) was dissolved into NaCl (150 mmol/L) solution, and coomassie brilliant blue (CBB, C-250) was added into ethyl alcohol (95%). Then 100 mL phosphoric acid (85% w/v) was added into the solution and diluted to 1000 mL. The samples were then boiled in Biotinylated Ladder (16 μL ultrapure water, 2 μL loading buffer, and 2 μL DTT) for 10 min. The Wes 12–230 kDa Master Kit with split buffer was loaded into the wells. The sample plates were centrifuged for 5 min at speed of 3000 rpm. Finally, the specimens were tested by protein simple western detector (WS-2494, ProteinSimple, California, USA). Separation gel, spacer gel, and samples were absorbed for 300 s, 15 s and 9 s, respectively. Electrophoresis was handled at 375 V for 25 min. Primary antibodies and second antibodies were incubated for 30 min. The luminous fluid was exposure reacted for 5–480 s. The Compass software (ProteinSimple, version 2.7.1) was used to analyze GFP protein expression values quantitatively.

2.10. Statistical analysis

The significance of statistical analysis was assessed using SPSS Statistics 17.0. All graphical data are shown as mean ± s.d. Significance levels were set at $^*p < 0.05$, $^{**}p < 0.01$, and $p < 0.05$ was considered statistically significant in the analysis.

3. Results and discussions

3.1. Characterization of short HNTs

Raw HNTs were firstly purified with standing for 24 h, and then the precipitate was abandoned. The suspension was centrifuged and freeze-dried. Subsequently, the purified HNTs were dispersed in PVP solution followed by sonication and centrifugation treatment. Fig. 2A shows SEM images of raw HNTs and short HNTs. Raw HNTs show diverse morphology with different length and diameter. The length of most of the nanotubes is longer than 200 nm. In contrast, the short HNTs emerge a smaller size especially the tube length. From the TEM morphology images (Fig. 2B), a difference in size is also distinguished. It can be seen that the typical tubular structure of HNTs with empty lumen is kept upon the shortening process. Short HNTs are all below 553 nm from the TEM images. Fig. 2C shows the particle size distribution of raw HNTs and short HNTs determined by DLS. The size of raw HNTs ranges from 78 nm to 1484 nm and short HNTs ranges from 45 nm to 553 nm. The hydrodynamic diameter (R_h) of short HNTs is 226.2 nm, while it is 365.6 nm of raw HNTs. The size below 200 nm of short HNTs occupies a proportion of 71.2% but that of the raw HNTs only occupies the proportion 37.2%. All these results indicate the successful reduction in size of HNTs by the sonication. In the shortening process, PVP acts the role of stabling the HNTs in the suspension due to the hydrogen bonding interactions between HNTs and PVP and provides the proper viscosity for the scission of tubes. In the presence of PVP, ultrasound as powerful energy can break the tube for getting short length. The size of short HNTs is proper for entering cells for drug or gene delivery [29,40,46]. No difference can be found in the FTIR

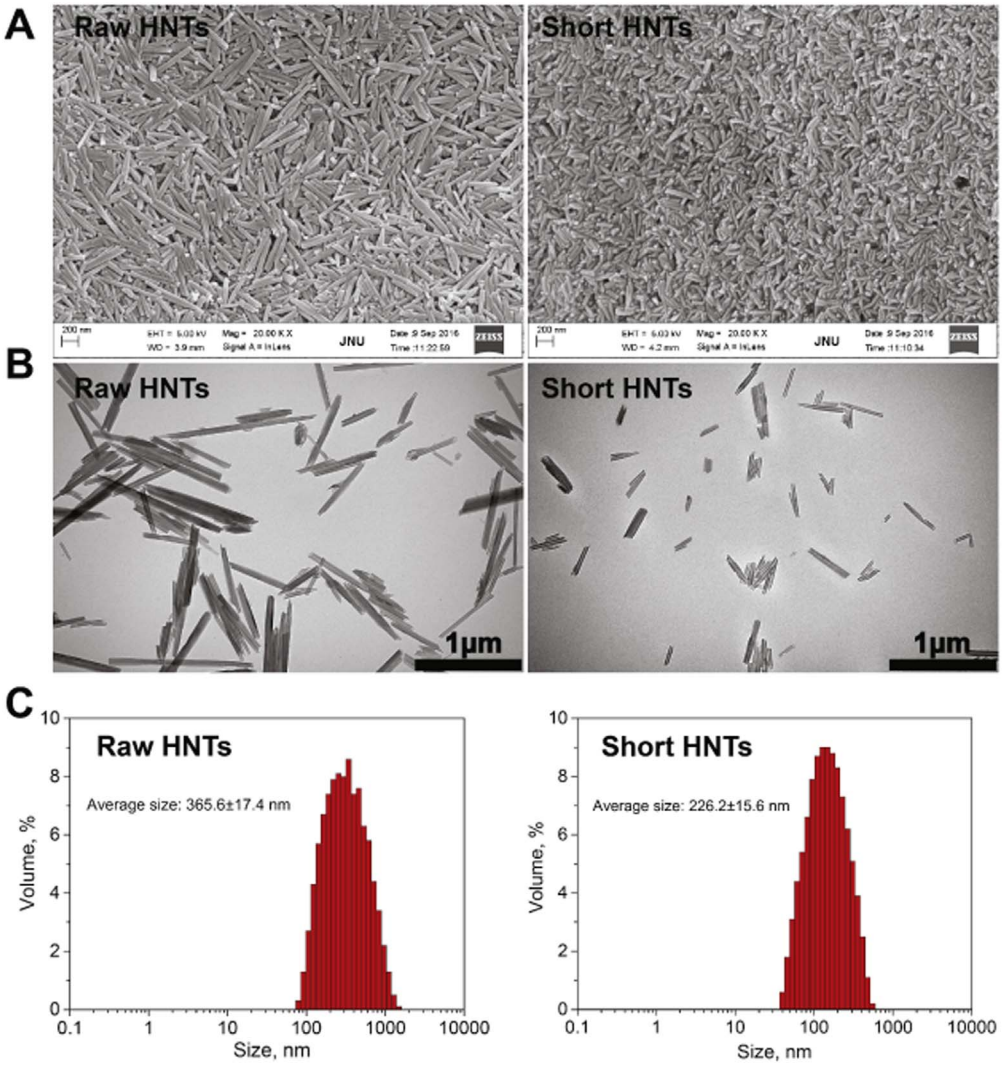

Fig. 2. SEM images (A), TEM images (B), and particle size distribution by DLS (C) of raw HNTs and short HNTs.

spectra for short HNTs and raw HNTs (Fig. S1), which means the shortening procedures do not change the chemical bonds of HNTs.

3.2. Synthesis and characterization of PEI-g-HNTs

The synthesis procedures for PEI-g-HNTs are shown in Fig. 3A. Firstly, HNTs-NH_2 were prepared by reacting the HNTs with APTES. Then, succinic anhydride was reacted with HNTs-NH_2 to produce HNTs-COOH. Finally, PEI-g-HNTs were obtained *via* condensation reactions between carboxyl groups in HNTs-COOH and amino groups in PEI using EDC/NHS as catalyzer. PEI10K was used for the nanotube modification owing to its strong binding to nucleic acids, effective uptake by cells, and the excellent proton sponge effect that triggers the endosomal release of DNA. Generally, cytotoxicity and transfection efficiency of PEI/DNA complex is depend on the molecular weight of PEI. PEI with a high molecular weight (such as 25 kDa) shows high transfection efficiency but it appears to be rather toxic towards cells compared to that with low molecular weight [47].

Fig. 3B shows TEM images of HNTs and PEI-g-HNTs. HNTs show tubular structure with empty lumen. PEI-g-HNTs also show tubular morphology with slightly different from short HNTs, and the typical empty lumen structure is reserved. So, the grafting processes do not harm the tubular structure and the dimension. As expected, PEI-g-HNTs show a layer of polymer around tubes outer surface, which is consistent with previous studies [48,49]. As shown in Fig. S2, if mixing PEI with HNTs *via* adsorption process, the free PEI or PEI escaped from HNTs would form small irregular shape, which will decrease the DNA loading efficacy and increase cytotoxicity. Fig. 3C shows AFM images of short HNTs and PEI-g-HNTs. A smooth and regular tube wall can be seen in the short HNTs image. In contrast, the surface of PEI-g-HNTs was coated with a thick layer PEI. For further studying the diameter changes, a diameter analysis was carried out on the AFM images of HNTs and PEI-g-HNTs (Fig. 3D). The diameter of fifty HNTs and PEI-g-HNTs from AFM images was analyzed. The results show that the mean diameter of HNTs is 42.38 nm while the value rises to 44.49 nm for the PEI-g-HNTs. So the calculated thickness of PEI layer round HNTs is ~2.11 nm. The morphology characterizations confirm the successful grafting of PEI on HNTs.

Fig. 4A show the UV spectrum of ninhydrin treated with different HNTs samples which illustrate the quantitative analysis of amine groups on HNTs surfaces. When treated with ninhydrin colorimetric assay, short HNTs show no color change and no absorbance peak at 570 nm, suggesting no amine groups in unmodified HNTs. The solution color of PEI treated ninhydrin solution turns into purple, while PEI-g-HNTs treated ninhydrin solution appears a slight purple color. The intensity of the absorbance peak at 570 nm is proportional to the amine density on the surfaces. The curve of PEI-g-HNTs treated ninhydrin solution lies between the curve of HNTs and PEI. This indicates amine groups are grafted onto HNTs. Fig. 4B compares the XRD pattern of PEI-g-HNTs and HNTs. After grafted with PEI, the typical (001) plane diffraction peak of HNTs at 12° slightly decreases, which suggests the shielding effect on the layer spacing of HNTs by the PEI

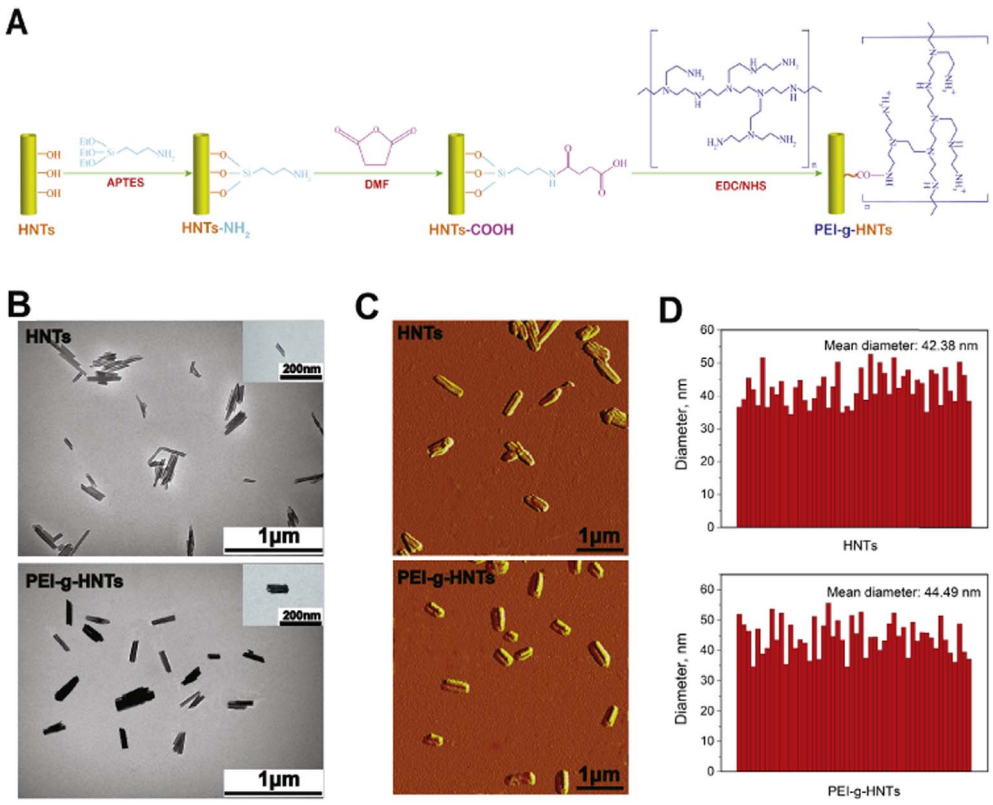

Fig. 3. Schematic illustration of the synthetic procedures for PEI-g-HNTs (A); TEM images (B), AFM images (C), and the size analysis (D) of HNTs and PEI-g-HNTs.

macromolecules chains. Fig. 4C shows the zeta potential of HNTs and PEI-g-HNTs. HNTs possess a negatively charged surface with a zeta potential of − 18.1 mV, while PEI-g-HNTs show a positively charged surface with zeta potential of + 26.9 mV. Therefore, the PEI-g-HNTs are easier to bind DNA and enter the cells compared with unmodified HNTs. Fig. 4D shows the FTIR spectra of HNTs, PEI and PEI-g-HNTs. HNTs show absorption peaks at 3695 cm^{-1} and 3625 cm^{-1}, which are assigned to the O—H stretching peak of inner-surface hydroxyl groups and O—H stretching vibration of hydroxyl groups, respectively. The peaks around 1016 cm^{-1} and 908 cm^{-1} are assigned to Si—O

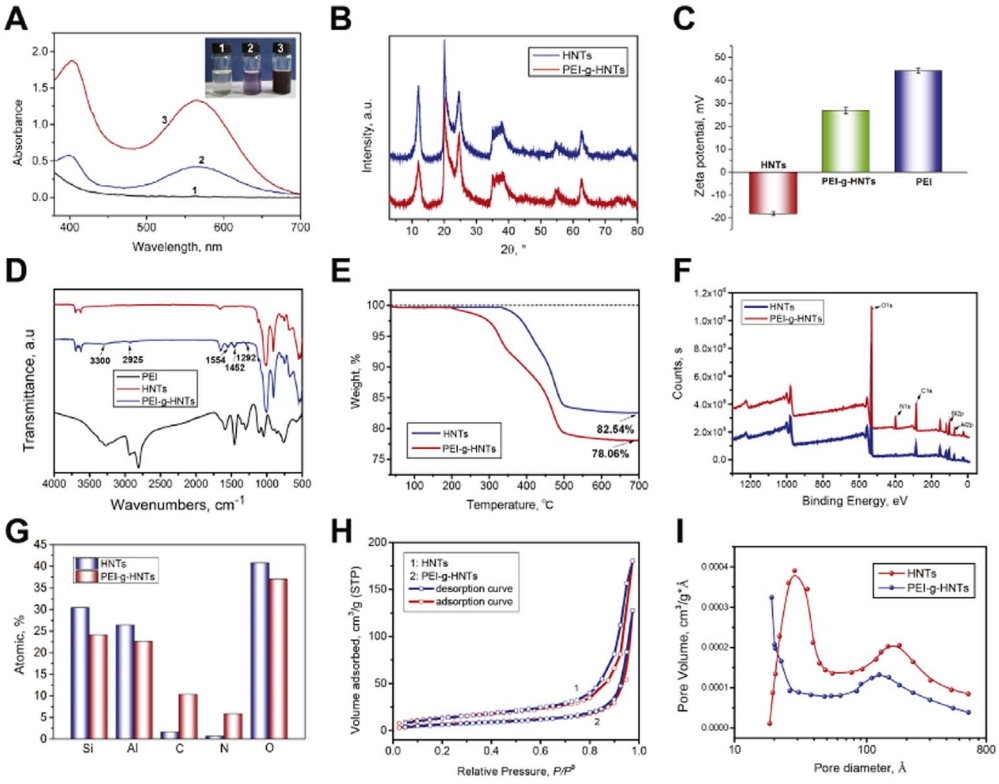

Fig. 4. Analysis of surface amine content of (1) HNTs, (2) PEI-g-HNTs, and (3) PEI using ninhydrin colorimetric assay (A); XRD pattern (B), zeta potential (C), FT-IR (D), thermogravimetric (E), XPS analysis (F), atomic ratio (G), nitrogen adsorption-desorption curves (H), BJH pore analysis (I) of HNTs and PEI-g-HNTs.

stretching peak and O—H deformation of inner hydroxyl groups of HNTs, respectively [20]. PEI-g-HNTs show characteristics absorptions of both HNTs and PEI. For example, bend vibrations of C—N bond in acylamide appear at around 1452 cm^{-1} and 1554 cm^{-1} [50], and the peak at 1292 cm^{-1} is attributed to C—N stretching vibration of the amine group. The peaks at 3300 cm^{-1} and 2935 cm^{-1} are ascribed to the N—H stretching vibration of the amine group and the C—H stretching vibration of PEI.

TGA curves of HNTs and PEI-g-HNTs are shown in Fig. 4E. PEI-g-HNTs have a weight loss of 21.94% from 30 to 700 °C, but HNTs only have 17.46% weight loss. The grafting ratio of PEI to HNTs is calculated to be 5.43%. Fig. 4F shows the XPS analysis of HNTs and PEI-g-HNTs. The intensity of $N1_s$ peak and $C1_s$ in the PEI-g-HNTs sample is obviously higher than that of HNTs. The atomic content of HNTs and PEI-g-HNTs (Fig. 4G) also suggests a significant increase of C and N content, which reflects the successful grafting of PEI on HNTs. It should be noticed that a few PVP can be adhered to the surface of HNTs (0.67% nitrogen content and 1.63% carbon content from XPS result) due to their strong interactions (mainly hydrogen bonding). However, little PVP cannot harm the tubular microstructures of HNTs and has little effect on the following cell experiment. Fig. 4H shows the nitrogen adsorption-desorption curves of HNTs and PEI-g-HNTs. At the same relative pressure, the value of desorption and adsorption value of PEI-g-HNTs is less than that of HNTs. That ascribes to that the grafted PEI on HNTs causes shielding effect which results in the slightly decreased adsorption ability of HNTs [41]. Fig. 4I shows BJH pore analysis of HNTs and PEI-g-HNTs. The peak at 3 nm is attributed to surface defects of HNTs [51], but the peak disappears after PEI grafting. Simultaneously, the total pore volume of PEI-g-HNTs is lower than that of HNTs. The pore analysis results also support the successful grafting of PEI on HNTs. These experiments were performed to demonstrae the composition in bulk and PEI grafting can be occured both inside and outside of the tubes. Especially, for the BJH pore analysis, it is clear that the part of PEI can be filled into the lumen of the tubes. Also, the TEM and AFM images of PEI-g-HNTs in Fig. 3 also demonstrate that the PEI layers are located both inside and outside of the tubes. However, it is generally considered that the location of PEI has little effect on the following gene loading and delivery experiment. In total, all the characterizations suggest the prepared PEI-g-HNTs can be used to bind DNA for cell transfection and drug delivery.

3.3. Biocompatibility and of characterization PEI-g-HNTs/pDNA complexes

Previous studies have shown the excellent cytocompatibility of HNTs, so they can be used to bind DNA as novel nanocarriers. Although pH value has a significant influence on the strutral stability of HNTs in corrosive environments. However, the intravesicular pH drops along the endocytic pathway, from pH 6.0–6.5 in early endosomes to pH 4.5–5.5 in late endosomes and lysosomes. Previous research has indicated < 1% of Al^{3+} and Si^{4+} of HNTs are dissolved even at a low pH of 2.38 after 50 days [52]. Therefore, the amount of leached metal ions of HNTs at the present cell culture condition is few and the influence of the metal ions on cells can be ignored.

AO/EB live/dead staining assay was carried out to confirm the cytotoxicity of PEI-g-HNTs/pDNA. AO can enter the live cells and staining the cell nucleus in a visible bright green color, while EB can enable the dead and late apoptosis cells shining with an orange color. The morphology of 293T cells (Fig. 5A) and HeLa cells (Fig. 5B) treated with PEI/pDNA and PEI-g-HNTs/pDNA complexes with different N/P ratios were observed using a fluorescence microscope. One can see that some 293T cells treated with PEI begin to show an orange color at the N/P ratio of 5, which indicates part of the cells is in apoptotic state. And the orange color of cells gradually becomes deep with the increase of N/P ratio, which suggests that, the cytotoxicity was gradually increased with the increase of N/P ratio. But there are not so many orange cells emerged for the PEI-g-HNTs group. At the N/P ratio of 40, almost no green cells emerge in the PEI/pDNA group, while most 293T cells are stained with green in the PEI-g-HNTs group, in the PEI-g-HNTs group. A similar phenomenon is happened to HeLa cells. At the N/P ratio of 20, cells treated with PEI/pDNA start to show discernible deep color. With the increase of N/P ratio, the cells were stained with deep color increased obviously. In contrast, the PEI-g-HNTs/pDNA groups show less cytotoxicity with the same N/P ratio even with high N/P ratio. At the N/P ratio of 20 and 40, HeLa cells only exhibit a slight red fluorescence signal. So, PEI-g-HNTs/pDNA have lower cell cytotoxicity than PEI/pDNA at the same N/P ratio.

Furthermore, CCK-8 assay was carried out to evaluate the *in vitro* cytotoxicity using 293T cells (Fig. 5C) and HeLa (Fig. 5D) cells. Before plotting, all the absorbance value results were normalized. It also can be seen that PEI/pDNA have a stronger toxicity than PEI-g-HNTs/pDNA at the same N/P ratio. For the 293T cells, the cell viability is decreased in both PEI/pDNA group and PEI-g-HNTs/pDNA group with the increase in N/P ratio. Especially, markedly decreased toxicity is noticed for the PEI-g-HNTs/pDNA group compared with PEI/pDNA group at N/P ratio of 40. The toxicity of PEI/pDNA increases with the increase of N/P ratio, while the relative cell viability of PEI-g-HNTs/pDNA group is still higher than 80% for all the N/P ratio. While for HeLa cells, the relative cell viability is slightly higher than 293T cells, which suggests HeLa cells have a stronger survivability. Similar to 293T cells group, cytotoxicity is gradually enhanced with the increase of N/P ratio. When the N/P ratio ranges from 5 to 40, the relative cell viability of both of PEI/pDNA group and PEI-g-HNTs group are gradually decreased. But the relative cell viability of PEI-g-HNTs/pDNA group still maintains a high level of 84.3%, while 75.2% in PEI/pDNA group at the N/P ratio of 40. Previous studies have reported that polycations such as PEI can bind with plasma membranes, which consequently induces cytotoxicity [53,54]. The nanoparticles can immobilize the macromolecular chains, which leads to the decrease in the cytotoxicity of cationic polymer since lowered density of cationic residues [55,56]. For example, PEI immobilized on GO sheets exhibited decreased cytotoxicity towards HeLa cells [47]. Hence, the decreased cytotoxicity of PEI-g-HNTs in the present work can also be ascribed to the decreased polymer cationic density on the HNTs surfaces.

As the PEI-g-HNTs/pDNA complexes are expected to deliver gene through intravenous injection in clinical. So, the blood compatibility of PEI-g-HNTs/pDNA was assessed by hemolysis analysis. If the hemolysis rate is below 5%, medical materials are considered as nonhemolysis according to national biological safety. Fig. 6A shows the hemolysis rate of PEI/pDNA and PEI-g-HNTs/pDNA at the N/P ratio of 20. The hemolysis rate of PEI/pDNA is 0.89%, while PEI-g-HNTs/pDNA shows hemolysis rate value of 1.79%. Although the hemolysis rate of PEI-g-HNTs/pDNA group is little higher than that of PEI/pDNA due to the effect of HNTs, PEI-g-HNTs can be used as a nanocarrier for drugs *in vivo* experiment for further study [57].

Zeta potential plays an important role in the cellular uptake of complexes. Zeta potentials of the complexes at different N/P ratios were then measured. As shown in Fig. 6C, the zeta potentials of PEI-g-HNTs/pDNA complexes increased from 12.2 mV to 19.3 mV with the increase of N/P ratio, which demonstrates that the ability of complexes binding DNA is enhanced with the increase of N/P ratio. To evaluate the effect of pH value on the stability of PEI-g-HNTs/pDNA complexes in the aqueous solution, zeta potentials of PEI-g-HNTs/pDNA complexes (N/P = 20) at the pH of 5.4, 7.4, 9 were also measured. Fig. 6E shows that zeta potentials of PEI-g-HNTs/pDNA maintain a stable value (~17 mV) with pH value increased from 5.4 to 9. Particle size is also a key factor affecting the cellular uptake rate of complexes. Fig. 6F reveals the size of PEI-g-HNTs/pDNA complexes (N/P = 20) at different pH value. With the changing of pH, the size of complexes is stable (~233 nm). The results illustrate the PEI-g-HNTs/pDNA complexes have a good stability in weak acid or weak base conditions. The diameters of the complexes at different N/P ratios were also compared. As shown in Fig. 6D, after binding with plasmid DNA, the size of the PEI-g-HNTs/

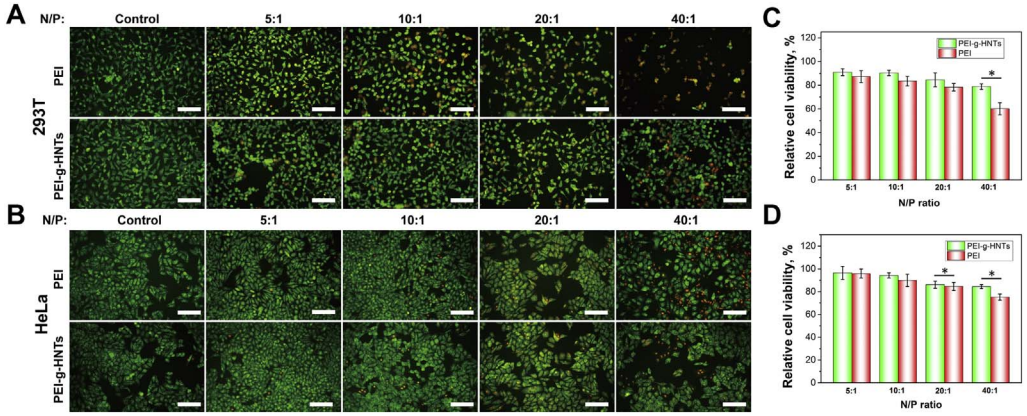

Fig. 5. The photos of AO/EB staining of 293T cells (A) and HeLa cells (B) treated with PEI/pDNA and PEI-g-HNTs/pDNA at the N/P ratios of 5, 10, 20, 40 for 24 h (the scale bars are 50 μm); relative viability of 293T cells (C) and HeLa cells (D) after being treated with PEI/pDNA and PEI-g-HNTs/pDNA after 24 h. Data are shown as means ± s.d. (n = 4). *, $p < 0.05$.

pDNA complexes slightly increases compared with PEI-g-HNTs (~226 nm).And the particle sizes of all the complexes slightly decreases with the increase of N/P ratio, which is related to the enhanced DNA condensation ability upon increase in N/P ratio. Furthermore, it can be seen from spectroscopic analysis that the characteristic absorbance peak of pDNA at 260 nm is still exist in PEI-g-HNTs/pDNA spectrum (Fig. S4), which suggests pDNA is bound with PEI-g-HNTs tightly. Fig. 5G shows the TEM images of PEI-g-HNTs/pDNA complexes at different N/P ratios. There is no obvious differences in morphology change with PEI-g-HNTs, which suggests the pDNA can be compacted into PEI-g-HNTs at various N/P ratios.

3.4. In vitro transfection

The transfection efficiency largely depends on the appropriate stability of nanoparticle/DNA complexes. The ability of the PEI-g-HNTs for binding pDNA was evaluated using gel electrophoresis retardation assay. As shown in Fig. 6B, PEI can entirely bind pDNA at the N/P ratio of equal to or higher than 2, indicating a strong binding ability of PEI to DNA. The PEI-g-HNTs can retard completely the electrophoretic mobility of pDNA when the N/P ratio is equal to or higher than 5. The difference is related to the much higher surface positive charge of PEI (+ 44.2 mV) compared with PEI-g-HNTs (+ 26.9 mV). From the gel electrophoresis result, both PEI and PEI-g-HNTs show good pDNA binding abilities at N/P ratios from 5 to 40 which are used to design the

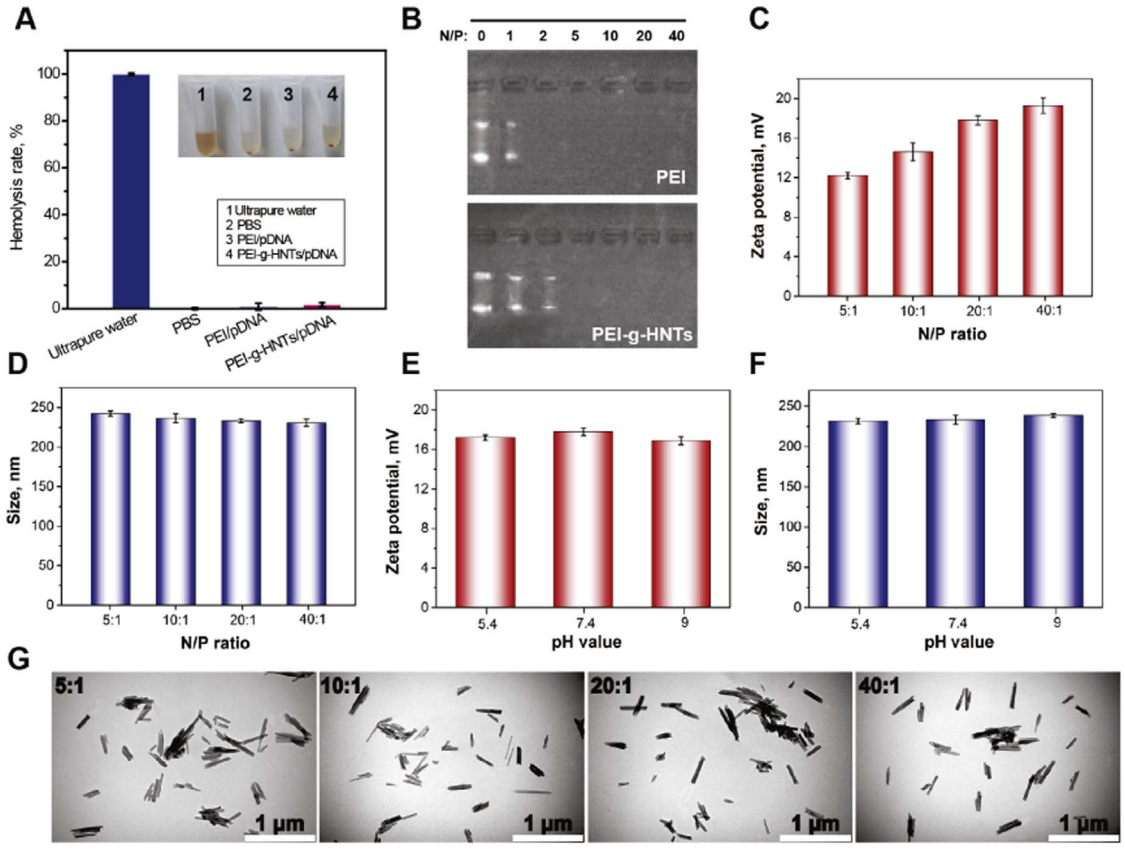

Fig. 6. Hemocompatibility of PEI/pDNA and PEI-g-HNTs/pDNA, ultrapure water (positive control), and PBS solution (negative control) (A); agarose gel electrophoresis retardation assay of pDNA complexed with PEI/pDNA and PEI-g-HNTs/pDNA at different N/P ratios, 0 represents naked pDNA (B); zeta potential (C) and mean particle size (D) of PEI-g-HNTs/pDNA complexes at various N/P ratios; zeta potential (E) and mean particle size (F) of PEI-g-HNTs/pDNA complexes (N/P = 20) at pH of 5.4, 7.4, 9;TEM images of PEI-g-HNTs/pDNA complexes at different N/P ratios (G).

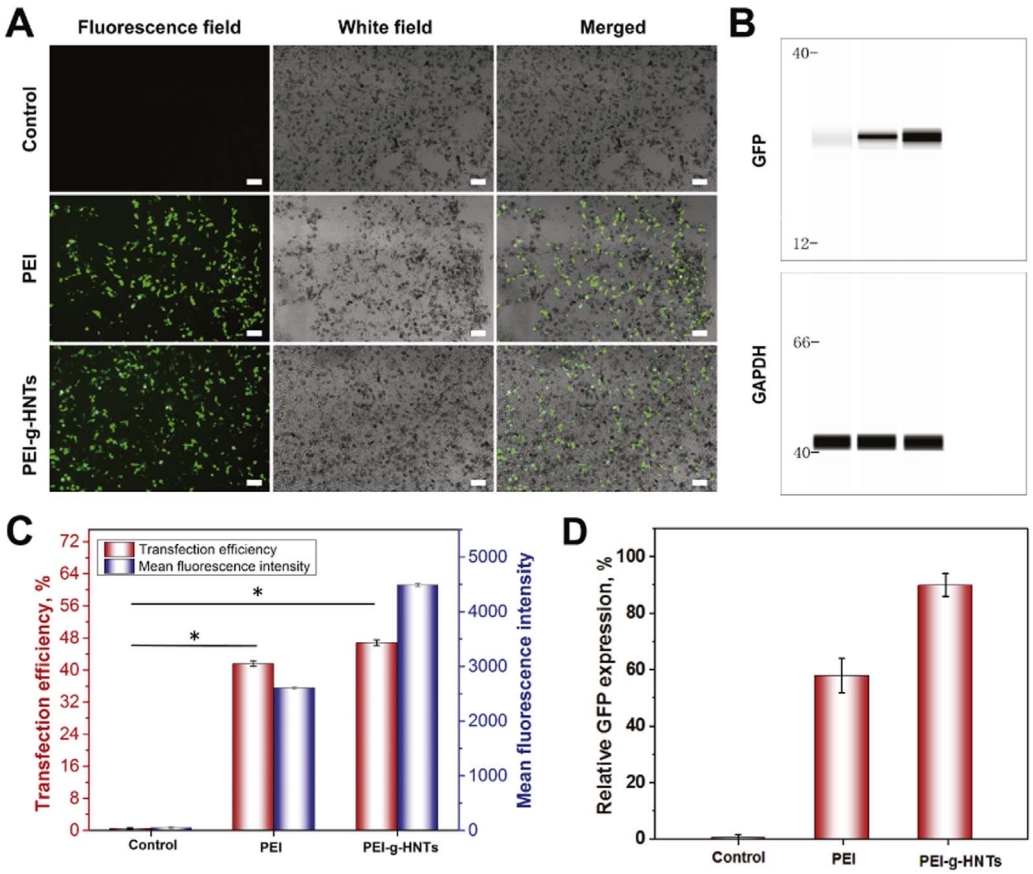

Fig. 7. The images of 293T cells of pDNA loaded PEI and PEI-g-HNTs (N/P ratio = 20) under fluorescence filed, white field and merged (under fluorescence filed and white field) field, the control group was the cells without addition any materials and gene (scale bars = 50 μm) (A); GFP transfection efficiency and mean fluorescence intensity of PEI/pDNA and PEI-g-HNTs/pDNA complex determined by flow cytometer at 72 h (C); representative GFP protein expression in 293T cells treated by PEI/pDNA and PEI-g-HNTs/pDNA complex determined by simple western immunoblots analysis (B); quantitative analysis of GFP protein expression as the ratio of area of GFP to area of glyceraldehyde-3-phosphate dehydrogenase (GAPDH) from simple western immunoblots results (D). Data are shown as means ± s.d. (n = 3). *, $p < 0.05$.

following experiments.

Fig. 7A shows the *in vitro* transfection photographs of PEI-g-HNTs/pDNA complex at the N/P ratio of 20. It can be seen the cells in the control group do not show any green fluoresce. For PEI/pDNA and PEI-g-HNTs/pDNA complexes group, many cells display green fluoresce, which suggests the GFP expression *via* gene transfection. PEI/pDNA complex could enter the cells after disassembly from HNTs if the PEI was only physically adsorbed on HNTs surfaces. However, the PEI was covalently grafted onto the HNTs in the present work, so the dissociation of PEI from HNTs was not easy. The fluorescence images of the transfection suggest the internalization of the PEI-g-HNTs/pDNA complex into cells and the PEI-g-HNTs can be used as nanovector of gene. The transfection efficiency and fluoresce intensity are further quantified by flow cytometry. As shown in Fig. 7C, PEI/pDNA complex shows a transfection efficiency of 41.6% after 72 h, while the PEI-g-HNTs/pDNA complex shows transfection efficiency of 46.8%. This suggests that the PEI-g-HNTs can effectively protect and delivery pDNA into cells as well as PEI. PEI-g-HNTs have proper nanoscale size (~200 nm) with unique needle-like morphology and positively charged surface, so they can be enter cell *via* endocytosis or penetrating the plasma membrane directly [20,33]. Simultaneously, the mean fluorescence intensity of PEI-g-HNTs/pDNA treated cells is 28.6% higher than that of PEI/pDNA treated cells. The low transfection efficacy and fluorescence intensity of PEI group may be attributed to the cytotoxicity as illustrate above. To further verify the transfection ability of PEI-g-HNTs/pDNA into 293T cells, the GFP expression quantity under the N/P ratio of 20 was analyzed by simple western immunoblots assay. As shown in Fig. 7B and D, PEI/pDNA group suffers a 32% reduction of GFP expression level than PEI-g-HNTs/pDNA group in 293T cells. The transfected 293T cells reserve its fission ability and show stable transfection for 72 h (Fig. S3). As a result, PEI-g-HNTs with low cytotoxicity and high transfection efficiency are promising candidate of non-viral gene vectors for gene therapy.

In order to study the possibility of PEI-g-HNTs as non-viral gene vectors for cancer therapy, the gene transfection efficiencies and GFP expression of PEI-g-HNTs/pDNA complex towards HeLa cells were analyzed. The HeLa cells cannot be transfected by the complex using the calcium phosphate transfection method. So electroporation transfection method was used to compare transfection effect of PEI-g-HNTs/pDNA and PEI/pDNA to HeLa cells at different N/P ratios. Fig. 8A shows the *in vitro* transfection fluorescence photographs of the two groups. It is clear that PEI-g-HNTs/pDNA complex shows a higher gene transfection efficacy than that of PEI/pDNA complex at the same N/P ratio. The transfection efficiency results (Fig. 8C) indicate that with the increase of N/P ratios (5 to 20), both the transfection efficiencies of PEI-g-HNTs/ pDNA complexes and PEI/pDNA complexes increase, but they are declined at N/P ratio of 40. The highest transfection efficiency is achieved at N/P ratio of 20 for both groups. The transfection efficiencies of PEI-g-HNTs/pDNA complex are reached to 44.4% at N/P = 20, while PEI/pDNA complex is only 36.6%. The transfection efficiencies of PEI-g-HNTs group are much higher than that of PEI group at all the designed N/P ratios. It is meaningful to compare the transfection efficiency to HeLa cells of the present work with previous reported gene carriers. The transfection efficiency using gold nanorods as a carrier of EGFP DNA was below 20% for HeLa cells [58]. Polyethylene glycol and polyethylenimine dual-functionalized graphene oxide could effectively transfect HeLa cells and showed maximum ~33.5% transfection efficiencies at N/P ratio = 10 [59]. Fe@carbon nanoparticles coated with LP-2000 lipid molecules showed ~75% gene transfection efficiencies in HeLa cells [60]. So, if the surface characters of HNTs can be further optimally designed, much higher transfection efficiency could be expected. Mean fluorescence intensity analyzed by flow cytometry (Fig. 8D) also shows the same trend. PEI-g-HNTs/pDNA complex possesses a higher value than that of PEI/pDNA complex at the same N/P ratio. With the increase of concentration N/P ratio, the mean fluorescence intensity of both PEI-g-HNTs/ pDNA complex and PEI/

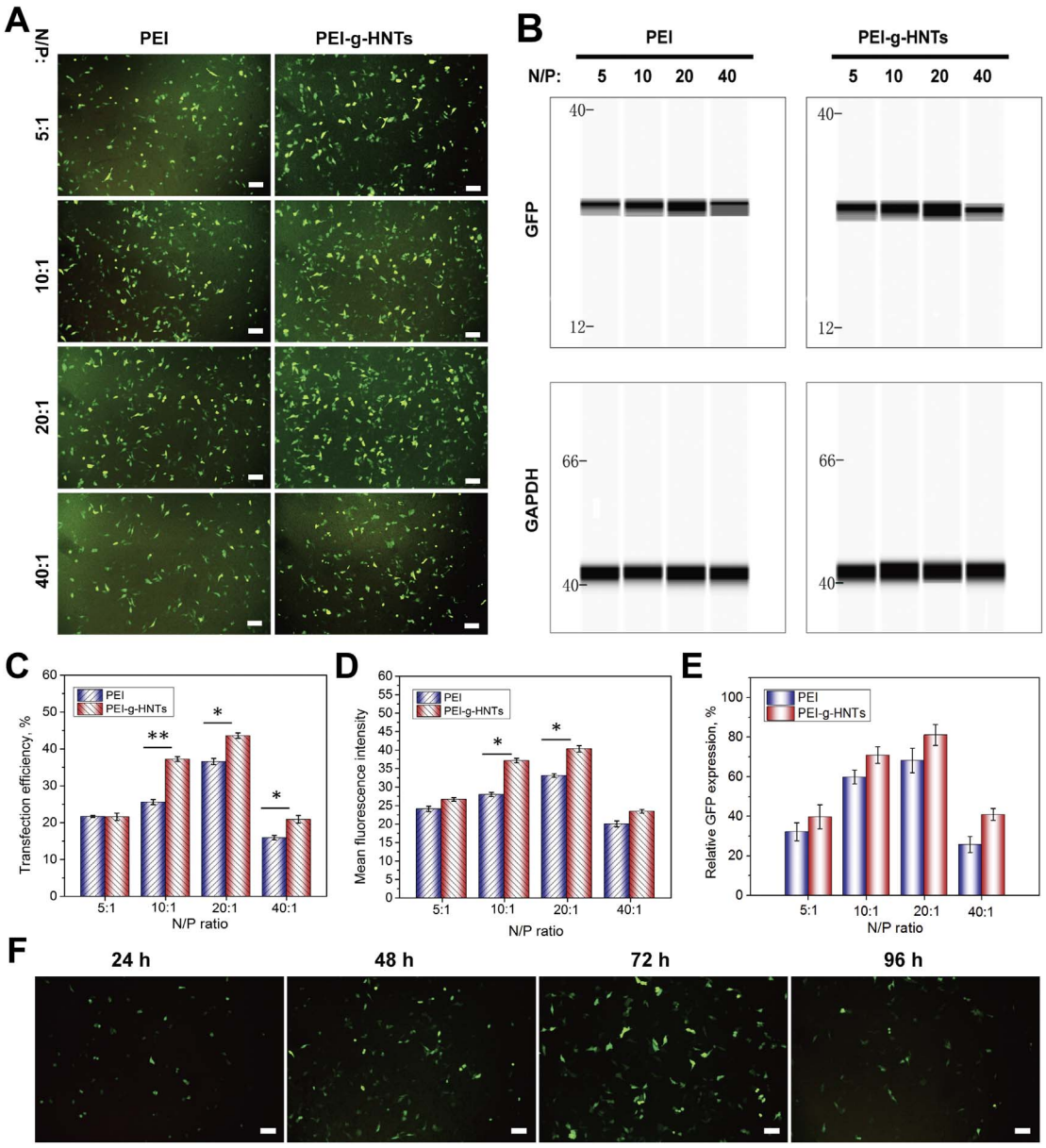

Fig. 8. The images of HeLa cells of pDNA loaded PEI and PEI-g-HNTs (N/P ratio = 5, 10, 20, 40) under fluorescence filed (scale bars = 50 μm) (A); GFP transfection efficiency (C), mean fluorescence intensity (D) of PEI/pDNA and PEI-g-HNTs/pDNA complex determined by flow cytometer at 72 h; representative GFP protein expression in HeLa cells treated by PEI/pDNA and PEI-g-HNTs/pDNA complex determined by simple western immunoblots (B); quantitative analysis of GFP protein expression as the ratio of area of GFP to area of GAPDH from simple western immunoblots results (E); fluorescent images of HeLa cells transfected with PEI-g-HNTs/pDNA complex (N/P = 20) after 24, 48, 72, and 96 h (F). Data are shown as means ± s.d. (n = 4). *, $p < 0.05$ and **, $p < 0$ 0.01.

pDNA complex increases. Also, the peak value of fluorescence intensity is found at the N/P ratio of 20, which suggests the ratio is most proper in the present system. Simple western immunoblots was carried out to detect GFP protein expression level. As shown in Fig. 8B and Fig. 8E, PEI/pDNA show less GFP expression at designed N/P ratios because of its relatively low transfection efficiency than PEI-g-HNTs/ pDNA complexes. Similar to the transfection efficiency results, the GFP protein expression levels of PEI-g-HNTs/pDNA and PEI/pDNA are higher at the N/P ratio of 20 than that at other N/P ratios.

Fig. 8F shows the fluorescent images of HeLa cells transfected with PEI-g-HNTs/pDNA complex (N/P = 20) after 24, 48, 72, and 96 h. After cells are transfected with complex from 24 to 72 h, more and more green cells appear. This suggests the sustainable release of pDNA from the complex occur with the contact time from 24 h to 72 h. The decreased green fluorescence at 96 h may be related to the death of the transfected cells. The pDNA release mechanism from PEI-g-HNTs/pDNA complex is proton sponge effect. When pH decreased from 7 to 5 in the lysosome, the grafted PEI will protonate and increase its hydrodynamic volume. This process causes the excessive amount of protons, which triggers the passive influx of chloride ions into the endosome and results in osmotic bursting of the endosomes. At the same time, the detachment of the negatively charged DNA from the nanoparticles complexes occurs and then the DNA is transported into the nucleus [61].

All the results indicate that PEI-g-HNTs exhibit good biocompatibility and high transfection efficiency, which shows promising application as novel non-viral gene delivery vehicles for gene therapy. Whether and how the PEI-g-HNTs work *in vivo* gene transfection needs further investigation. Also, the length of the short HNTs should be further homogenized to increase endocytosis efficiency and decrease the cytotoxicity, which will be reported in the future studies.

4. Conclusions

A novel non-viral gene vector based on HNTs for loading and delivering of pDNA has been developed. The ultrasonic treatment was used to cut the long HNTs into short nanotubes with 71.2% tubes smaller than 200 nm from DLS data. Then PEI was chemically grafted onto the HNTs to change the surface potential into positive charges. Morphological, physical, and chemical characterizations all confirm the successful grafting of HNTs by PEI. The *in vitro* cytotoxicity assays show PEI-g-HNTs/pDNA are less toxic to cells than PEI/pDNA, and PEI-g-HNTs/pDNA show a reasonable blood compatibility. The *in vitro* transfection results demonstrate PEI-g-HNTs/pDNA complex exhibits increased transfection efficiency and fluorescence intensity compares with PEI/pDNA complex towards 293T and HeLa cells. The transfection efficiencies of PEI-g-HNTs/pDNA complex towards HeLa cell can reach to 44.4% at N/P ratio of 20. GFP protein expression levels of PEI-g-HNTs/pDNA at the N/P ratio of 20 are higher than other N/P ratios. As PEI-g-HNTs vectors exhibit effective intracellular transporting and high transfection efficiency with low cytotoxicity, the prepared PEI-g-HNTs show promising application in gene therapy towards many diseases such as cancer.

Acknowledgments

This work was supported by the National High Technology Research and Development Program of China (grant number 2015AA020915), the National Natural Science Foundation of China (grant numbers 51473069, 51502113), and the Guangdong Natural Science Funds for Distinguished Young Scholar (grant number S2013050014606), Science and Technology Planning Project of Guangdong Province (grant number 2014A020217006), Guangdong Special Support Program (grant number 2014TQ01C127), and the Pearl River S & T Nova Program of Guangzhou (grant number 201610010026).

Appendix A. Supplementary data

Supplementary data to this article can be found online at http://dx.doi.org/10.1016/j.msec.2017.07.035.

References

[1] K. Wang, F.M. Kievit, M. Zhang, Nanoparticles for cancer gene therapy: recent advances, challenges, and strategies, Pharmacol. Res. 114 (2016) 56–66.
[2] J. Zhou, J. Liu, C.J. Cheng, T.R. Patel, C.E. Weller, J.M. Piepmeier, Z. Jiang, W.M. Saltzman, Biodegradable poly (amine-co-ester) terpolymers for targeted gene delivery, Nat. Mater. 11 (2012) 82–90.
[3] Z. Huang, Y.-M. Zhang, Q. Cheng, J. Zhang, Y.-H. Liu, B. Wang, X.-Q. Yu, Structure–activity relationship studies of symmetrical cationic bolasomes as non-viral gene vectors, J. Mater. Chem. B 4 (2016) 5575–5584.
[4] N. Cartier, S. Hacein-Bey-Abina, C.C. Bartholomae, G. Veres, M. Schmidt, I. Kutschera, M. Vidaud, U. Abel, L. Dal-Cortivo, L. Caccavelli, Hematopoietic stem cell gene therapy with a lentiviral vector in X-linked adrenoleukodystrophy, Science 326 (2009) 818–823.
[5] B. Wang, W.-J. Yi, J. Zhang, Q.-F. Zhang, M.-M. Xun, X.-Q. Yu, TACN-based cationic lipids with amino acid backbone and double tails: materials for non-viral gene delivery, Med. Chem. Lett. 24 (2014) 1771–1775.
[6] E. Ye, X.J. Loh, Polymeric hydrogels and nanoparticles: a merging and emerging field, Aust. J. Chem. 66 (2013) 997–1007.
[7] R. Lakshminarayanan, E.O. Chi-Jin, X.J. Loh, R.M. Kini, S. Valiyaveettil, Purification and characterization of a vaterite-inducing peptide, pelovaterin, from the eggshells of *Pelodiscus sinensis* (Chinese soft-shelled turtle), Biomacromolecules 6 (2005) 1429–1437.
[8] R. Lakshminarayanan, X.J. Loh, S. Gayathri, S. Sindhu, Y. Banerjee, R.M. Kini, S. Valiyaveettil, Formation of transient amorphous calcium carbonate precursor in quail eggshell mineralization: an in vitro study, Biomacromolecules 7 (2006) 3202–3209.
[9] X.J. Loh, T.-C. Lee, Q. Dou, G.R. Deen, Utilising inorganic nanocarriers for gene delivery, Biomater. Sci. 4 (2016) 70–86.
[10] Q.Q. Dou, C.P. Teng, E. Ye, X.J. Loh, Effective near-infrared photodynamic therapy assisted by upconversion nanoparticles conjugated with photosensitizers, Int. J. Nanomedicine 10 (2015) 419.
[11] E. Ye, M.D. Regulacio, M.S. Bharathi, H. Pan, M. Lin, M. Bosman, K.Y. Win, H. Ramanarayan, S.-Y. Zhang, X.J. Loh, An experimental and theoretical investigation of the anisotropic branching in gold nanocrosses, Nano 8 (2016) 543–552.
[12] H.C. Guo, E. Ye, Z. Li, M.-Y. Han, X.J. Loh, Recent progress of atomic layer deposition on polymeric materials, Mater. Sci. Eng. C 70 (2017) 1182–1191.
[13] B.M. Teo, D.J. Young, X.J. Loh, Magnetic anisotropic particles: toward remotely actuated applications, Part. Part. Syst. Charact. (2016).
[14] P. LináChee, X. JunáLoh, Multi-functional fluorescent carbon dots with antibacterial and gene delivery properties, RSC Adv. 5 (2015) 46817–46822.
[15] C. Dhand, N. Dwivedi, X.J. Loh, A.N.J. Ying, N.K. Verma, R.W. Beuerman, R. Lakshminarayanan, S. Ramakrishna, Methods and strategies for the synthesis of diverse nanoparticles and their applications: a comprehensive overview, RSC Adv. 5 (2015) 105003–105037.
[16] Z. Li, E. Ye, R. Lakshminarayanan, X.J. Loh, Recent advances of using hybrid nanocarriers in remotely controlled therapeutic delivery, Small (2016) DOI.
[17] K. Huang, Q. Dou, X.J. Loh, Nanomaterial mediated optogenetics: opportunities and challenges, RSC Adv. 6 (2016) 60896–60906.
[18] L. Zhang, Z. Lu, Q. Zhao, J. Huang, H. Shen, Z. Zhang, Enhanced chemotherapy efficacy by sequential delivery of siRNA and anticancer drugs using PEI-grafted graphene oxide, Small 7 (2011) 460–464.
[19] C. Caoduro, E. Hervouet, C. Girard-Thernier, T. Gharbi, H. Boulahdour, R. Delage-Mourroux, M. Pudlo, Carbon nanotubes as gene carriers: focus on internalization pathways related to functionalization and properties, Acta Biomater. (2016).
[20] J. Yang, Y. Wu, Y. Shen, C. Zhou, Y.-F. Li, R.-R. He, M. Liu, Enhanced therapeutic efficacy of doxorubicin for breast cancer using chitosan oligosaccharide-modified halloysite nanotubes, ACS Appl. Mater. Interfaces 8 (2016) 26578–26590.
[21] N.L. Rosi, D.A. Giljohann, C.S. Thaxton, A.K. Lytton-Jean, M.S. Han, C.A. Mirkin, Oligonucleotide-modified gold nanoparticles for intracellular gene regulation, Science 312 (2006) 1027–1030.
[22] M. Cruz-Acuña, L. Maldonado-Camargo, J. Dobson, C. Rinaldi, From oleic acid-capped iron oxide nanoparticles to polyethyleneimine-coated single-particle magnetofectins, J. Nanopart. Res. 18 (2016) 268.
[23] W. Park, H.N. Yang, D. Ling, H. Yim, K.S. Kim, T. Hyeon, K. Na, K.-H. Park, Multimodal transfection agent based on monodisperse magnetic nanoparticles for stem cell gene delivery and tracking, Biomaterials 35 (2014) 7239–7247.
[24] M. Yu, Y. Niu, J. Zhang, H. Zhang, Y. Yang, E. Taran, S. Jambhrunkar, W. Gu, P. Thorn, C. Yu, Size-dependent gene delivery of amine-modified silica nanoparticles, Nano Res. 9 (2016) 291–305.
[25] M. Liu, Y. Chang, J. Yang, Y. You, R. He, T. Chen, C. Zhou, Functionalized halloysite nanotube by chitosan grafting for drug delivery of curcumin to achieve enhanced anticancer efficacy, J. Mater. Chem. B 4 (2016) 2253–2263.
[26] E. Joussein, S. Petit, J. Churchman, B. Theng, D. Righi, B. Delvaux, Halloysite clay minerals–a review, Clay Miner. 40 (2005) 383–426.
[27] Y.M. Lvov, D.G. Shchukin, H. Mohwald, R.R. Price, Halloysite clay nanotubes for controlled release of protective agents, ACS Nano 2 (2008) 814–820.
[28] M. Liu, Y. Zhang, C. Wu, S. Xiong, C. Zhou, Chitosan/halloysite nanotubes bionanocomposites: structure, mechanical properties and biocompatibility, Int. J. Biol. Macromol. 51 (2012) 566–575.
[29] M. Liu, Z. Jia, D. Jia, C. Zhou, Recent advance in research on halloysite nanotubes-polymer nanocomposite, Prog. Polym. Sci. 39 (2014) 1498–1525.
[30] Y. Lvov, E. Abdullayev, Functional polymer–clay nanotube composites with sustained release of chemical agents, Prog. Polym. Sci. 38 (2013) 1690–1719.
[31] Y. Lvov, W. Wang, L. Zhang, R. Fakhrullin, Halloysite clay nanotubes for loading and sustained release of functional compounds, Adv. Mater. 28 (2016) 1227–1250.
[32] Y.-F. Shi, Z. Tian, Y. Zhang, H.-B. Shen, N.-Q. Jia, Functionalized halloysite nanotube-based carrier for intracellular delivery of antisense oligonucleotides, Nanoscale Res. Lett. 6 (2011) 1.
[33] H. Wu, Y. Shi, C. Huang, Y. Zhang, J. Wu, H. Shen, N. Jia, Multifunctional nanocarrier based on clay nanotubes for efficient intracellular siRNA delivery and gene silencing, J. Biomater. Appl. 28 (2014) 1180–1189.
[34] R.L. Frost, J. Kristof, Intercalation of halloysite: a Raman spectroscopic study, Clay Clay Miner. 45 (1997) 551–563.
[35] N.G. Veerabadran, R.R. Price, Y.M. Lvov, Clay nanotubes for encapsulation and sustained release of drugs, Nano 2 (2007) 115–120.
[36] N.G. Veerabadran, D. Mongayt, V. Torchilin, R.R. Price, Y.M. Lvov, Organized shells on clay nanotubes for controlled release of macromolecules, Macromol. Rapid Commun. 30 (2009) 99–103.
[37] M. Liu, R. He, J. Yang, W. Zhao, C. Zhou, Stripe-like clay nanotubes patterns in glass capillary tubes for capture of tumor cells, ACS Appl. Mater. Interfaces 8 (2016) 7709–7719.
[38] R. Rong, X. Xu, S. Zhu, B. Li, X. Wang, K. Tang, Facile preparation of homogeneous and length controllable halloysite nanotubes by ultrasonic scission and uniform viscosity centrifugation, Chem. Eng. J. 291 (2016) 20–29.
[39] S.E. Gratton, P.A. Ropp, P.D. Pohlhaus, J.C. Luft, V.J. Madden, M.E. Napier, J.M. DeSimone, The effect of particle design on cellular internalization pathways, Proc. Natl. Acad. Sci. U. S. A. 105 (2008) 11613–11618.
[40] Y. Sato, A. Yokoyama, K.-i. Shibata, Y. Akimoto, S.-I. Ogino, Y. Nodasaka, T. Kohgo, K. Tamura, T. Akasaka, M. Uo, Influence of length on cytotoxicity of multi-walled carbon nanotubes against human acute monocytic leukemia cell line THP-1 in vitro and subcutaneous tissue of rats in vivo, Mol. BioSyst. 1 (2005) 176–182.
[41] M. Liu, B. Guo, Q. Zou, M. Du, D. Jia, Interactions between halloysite nanotubes and 2, 5-bis (2-benzoxazolyl) thiophene and their effects on reinforcement of polypropylene/halloysite nanocomposites, Nanotechnology 19 (2008) 205709.
[42] Y. Joo, Y. Jeon, S.U. Lee, J.H. Sim, J. Ryu, S. Lee, H. Lee, D. Sohn, Aggregation and stabilization of carboxylic acid functionalized halloysite nanotubes (HNT-COOH), J. Phys. Chem. C 116 (2012) 18230–18235.
[43] B. Chertok, A.E. David, V.C. Yang, Polyethyleneimine-modified iron oxide

nanoparticles for brain tumor drug delivery using magnetic targeting and intra-carotid administration, Biomaterials 31 (2010) 6317–6324.
[44] Z. Liu, G. Song, C. Zou, G. Liu, W. Wu, T. Yuan, X. Liu, Acrylamide induces mitochondrial dysfunction and apoptosis in BV-2 microglial cells, Free Radic. Biol. Med. 84 (2015) 42–53.
[45] J.A. Dahl, I. Jung, H. Aanes, G.D. Greggains, A. Manaf, M. Lerdrup, G. Li, S. Kuan, B. Li, A.Y. Lee, Broad histone H3K4me3 domains in mouse oocytes modulate maternal-to-zygotic transition, Nature (2016).
[46] K. Kostarelos, L. Lacerda, G. Pastorin, W. Wu, S. Wieckowski, J. Luangsivilay, S. Godefroy, D. Pantarotto, J.-P. Briand, S. Muller, Cellular uptake of functionalized carbon nanotubes is independent of functional group and cell type, Nat. Nanotechnol. 2 (2007) 108–113.
[47] L. Feng, S. Zhang, Z. Liu, Graphene based gene transfection, Nano 3 (2011) 1252–1257.
[48] M. Liu, C. Wu, Y. Jiao, S. Xiong, C. Zhou, Chitosan–halloysite nanotubes nanocomposite scaffolds for tissue engineering, J. Mater. Chem. B 1 (2013) 2078–2089.
[49] B. Mu, M. Zhao, P. Liu, Halloysite nanotubes grafted hyperbranched (co) polymers via surface-initiated self-condensing vinyl (co) polymerization, J. Nanopart. Res. 10 (2008) 831–838.
[50] T.A. Saleh, M. Tuzen, A. Sarı, Polyethylenimine modified activated carbon as novel magnetic adsorbent for the removal of uranium from aqueous solution, Chem. Eng. Res. Des. 117 (2017) 218–227.
[51] M. Liu, B. Guo, M. Du, X. Cai, D. Jia, Properties of halloysite nanotube–epoxy resin hybrids and the interfacial reactions in the systems, Nanotechnology 18 (2007) 455703.
[52] R.D. White, D.V. Bavykin, F.C. Walsh, The stability of halloysite nanotubes in acidic and alkaline aqueous suspensions, Nanotechnology 23 (2012) 065705.
[53] C. Brunot, L. Ponsonnet, C. Lagneau, P. Farge, C. Picart, B. Grosgogeat, Cytotoxicity of polyethyleneimine (PEI), precursor base layer of polyelectrolyte multilayer films, Biomaterials 28 (2007) 632–640.
[54] O. Boussif, F. Lezoualc'h, M.A. Zanta, M.D. Mergny, D. Scherman, B. Demeneix, J.-P. Behr, A versatile vector for gene and oligonucleotide transfer into cells in culture and in vivo: polyethylenimine, Proc. Natl. Acad. Sci. U. S. A. 92 (1995) 7297–7301.
[55] D. Putnam, C.A. Gentry, D.W. Pack, R. Langer, Polymer-based gene delivery with low cytotoxicity by a unique balance of side-chain termini, Proc. Natl. Acad. Sci. 98 (2001) 1200–1205.
[56] J. Zhu, A. Tang, L.P. Law, M. Feng, K.M. Ho, D.K. Lee, F.W. Harris, P. Li, Amphiphilic core-shell nanoparticles with poly (ethylenimine) shells as potential gene delivery carriers, Bioconjug. Chem. 16 (2005) 139–146.
[57] H.-Y. Liu, L. Du, Y.-T. Zhao, W.-Q. Tian, In vitro hemocompatibility and cytotoxicity evaluation of halloysite nanotubes for biomedical application, J. Nanomater. 16 (2015) 384.
[58] C.-C. Chen, Y.-P. Lin, C.-W. Wang, H.-C. Tzeng, C.-H. Wu, Y.-C. Chen, C.-P. Chen, L.-C. Chen, Y.-C. Wu, DNA-gold nanorod conjugates for remote control of localized gene expression by near infrared irradiation, J. Am. Chem. Soc. 128 (2006) 3709–3715.
[59] L. Feng, X. Yang, X. Shi, X. Tan, R. Peng, J. Wang, Z. Liu, Polyethylene glycol and polyethylenimine dual-functionalized nano-graphene oxide for photothermally enhanced gene delivery, Small 9 (2013) 1989–1997.
[60] R. Vankayala, C.-S. Chiang, J.-I. Chao, C.-J. Yuan, S.-Y. Lin, K.C. Hwang, A general strategy to achieve ultra-high gene transfection efficiency using lipid-nanoparticle composites, Biomaterials 35 (2014) 8261–8272.
[61] M. Feng, D. Lee, P. Li, Intracellular uptake and release of poly (ethyleneimine)-co-poly (methyl methacrylate) nanoparticle/pDNA complexes for gene delivery, Int. J. Pharm. 311 (2006) 209–214.